Q. J. R. Meteorol. Soc. (2005), **131**, pp. 2313–2336 doi: 10.1256/qj.04.44

Mode decomposition as a methodology for developing convective-scale representations in global models

By JUN-ICHI YANO[1]†, JEAN-LUC REDELSPERGER[1], PETER BECHTOLD[2] and FRANÇOISE GUICHARD[1]

[1]*CNRM–GAME, Météo-France and CNRS, 31057 Toulouse Cedex, France*
[2]*ECMWF, Shinfield Park, Reading, RG2 9AX, UK*

(Received 15 March 2004; revised 13 April 2005)

SUMMARY

Mode decomposition is proposed as a methodology for developing subgrid-scale physical representations in global models by a systematic reduction of an originally full system such as a cloud-resolving model (CRM). A general formulation is presented, and also discussed are mathematical requirements that make this procedure possible. Features of this general methodology are further elucidated by the two specific examples: mass fluxes and wavelets.

The traditional mass-flux formulation for convective parametrizations is derived as a special case from this general formulation. It is based on the decomposition of a horizontal domain into an approximate sum of piecewise-constant segments. Thus, a decomposition of CRM outputs on this basis is crucial for their direct verification. However, this decomposition is mathematically not well-posed nor unique due to the lack of *admissibility*. A classification into cloud types, primarily based on precipitation characteristics of the atmospheric columns, that has been used as its substitute, does not necessarily provide a good approximation for a piecewise-constant segment decomposition. This difficulty with mass-flux decomposition makes a verification of the formulational details of parametrizations based on mass fluxes by a CRM inherently difficult.

The wavelet decomposition is an alternative possibility that can more systematically decompose the convective system. Its completeness and orthogonality also allow a *prognostic* description of a CRM system in wavelet space in the same manner as is done in Fourier space. The wavelets can, furthermore, efficiently represent the various convective coherencies by a limited number of modes due to their spatial localizations. Thus, the degree of complexity of the wavelet-based *prognostic* representation of a CRM can be extensively reduced. Such an extensive reduction *may* allow its use in place of current cumulus parametrizations. This wavelet-based scheme can easily be verified from the full original system due to its direct reduction from the latter. It also fully takes into account the multi-scale nonlinear interactions, unlike the traditional mass-flux-based schemes.

KEYWORDS: Cloud-resolving model Cumulus parametrization Mass flux Wavelets

1. INTRODUCTION

The subgrid-scale physical representation (normally called the parametrization) is a major source of uncertainties in current global climate modelling. As it stands, different physical processes in subgrid scales are represented separately by different schemes, without much consideration of mutual consistency. As emphasized in a recent review by Arakawa (2004), a unified description of these subgrid-scale physical processes is obviously what is needed. Such a unified description would become possible if the originally full physical system could be systematically and extensively reduced into a simpler system. The present paper proposes mode decomposition as a general methodology for this purpose. As an example of a full physical system, we take the cloud-resolving model (CRM), keeping particularly in mind the convective-scale processes that are traditionally represented by cumulus parametrizations.

The CRM has widely been recognized as a promising tool for developing and verifying cumulus parametrizations (Browning *et al.* 1993; Moncrieff *et al.* 1997; Redelsperger *et al.* 2000) since the pioneering work by Gregory and Miller (1989). Ability of CRMs to model realistic atmospheric deep convection has been established

† Corresponding author: CNRM–GAME, Météo-France, 42 av. Coriolis, 31057 Toulouse Cedex, France.
e-mail: yano@cnrm.meteo.fr

(Soong and Tao 1980; Lafore *et al.* 1988; Xu and Randall 1996; Grabowski *et al.* 1996, 1998; Guichard *et al.* 1997, 2000; Wu *et al.* 1998, 1999; Donner *et al.* 1999; Wu and Moncrieff 2001). Comparisons of performance between CRMs and parametrizations have already been extensively investigated in terms of 'grid-box' averaged statistics (Xu and Arakawa 1992; Xu *et al.* 1992; Xu 1994, 1995; Alexander and Cotton 1998; Gray 2000; Xu and Randall 2001; Gregory and Guichard 2002). Here, 'grid-box' corresponds to a horizontal grid-box for the global models, and also at the same time the horizontal modelling domain for a CRM.

When a CRM is run over such a 'grid-box' domain, these simulations should also allow more direct evaluations of various hypotheses within cumulus parametrizations, especially those of the closure hypotheses, which have not been hitherto much attempted. Such direct evaluations are much facilitated when a cumulus parametrization is constructed by a systematic reduction from an originally full system such as a CRM. Then the individual steps of the reduction can be retrospectively verified by CRM simulations.

The present work is partially inspired by the idea of a more direct use of a CRM in global models, originally proposed by Grabowski and Smolarkiewicz (1999), and reviewed by Randall *et al.* (2003). Obviously, the problem of the subgrid-scale parametrization would simply disappear if a high-resolution model, that computes the subgrid-scale physical processes explicitly, were placed at each grid box of a global model. With the increase of computing power, in fact, it is possible to place a small-size CRM at each grid box of a low-resolution global model, which is the core of their proposal.

In turn, the present paper asks how a CRM can lead to a *more efficient* subgrid-scale representation by its systematic reduction, and suggests how a parametrization can be verified under the given reduction framework. Mode decomposition is a general mathematical methodology for describing a physical system by a set of functions (or modes) in both a diagnostic and prognostic manner. The Fourier decomposition is the best known mathematical example, but more importantly, the mass-flux formulation developed by Ooyama (1971), and by Arakawa and Schubert (1974), can also be considered as belonging to this category†.

Once a mode decomposition is properly applied on a given physical system, any evolution of the system is described by that of the coefficients for the adopted set of modes. Furthermore, if a limited number of modes can approximate the original full system well, computations for evolution of these modes are sufficient for describing the evolution of the latter. Thus, such a highly truncated model can be used as a representation of subgrid-scale physical processes in global models. The representation scheme may further be simplified by introducing various approximations, leading to a *parametric* representation of subgrid-scale physical processes, or a *parametrization*. Most of the current parametrizations are *diagnostic* by assuming an instantaneous adjustment by these processes. What is called *closure* becomes necessary in order to enable such a parametric representation.

Arakawa and Schubert's (1974) mass-flux formulation may be considered as the previous best effort for providing such a general framework. However, even 30 years

† Strictly speaking, the mass flux is defined solely as an integration of the vertical mass transport over a convective area (cf. Eq. (2) of Arakawa and Schubert 1974). No additional constraint is posed in the original work by Arakawa and Schubert (1974). In this respect, the mass-flux formulation is re-derived in the present paper under stronger constraints of a mode decomposition. Thus, although mathematically equivalent results are obtained, physical interpretations that follow may not be equivalent to those of Arakawa and Schubert (A. Arakawa 2005, personal communication).

after this benchmark work, the progress of the convective representation is slow (cf. Randall *et al.* 2003). A more general theoretical framework that allows systematic constructions and verifications of the subgrid-scale parametrization is clearly needed.

An alternative general methodology, that is extensively used in atmospheric boundary-layer parametrizations, is the moment expansion (e.g. Mellor and Yamada 1974; Stull 1993). Under this framework, an adapted closure for a parametrization can be verified by directly evaluating the moments from CRM simulations. This approach is applicable to the inertial range of the spectrum of turbulent flows where a horizontal homogeneity can be assumed. But it is not quite applicable to deep moist convection, which is associated with isolated draughts and organized structures, although basic turbulent scalings are currently explored (cf. Grant and Brown 1999; Khairoutdinov and Randall 2002; Grant and Lock 2004).

The present paper does not propose any specific procedures for a parametrization development. However, importantly, any parametrization developed from a specific procedure can be systematically verified by direct modelling of a full system for every step of reductions including the closure hypotheses, if it follows the general framework proposed by the present paper. By including the mass-flux formulation as its special case, the present paper further indicates that all the parametrizations developed under this formulation can potentially be verified systematically by direct modellings, but with a major caveat.

The next section briefly reviews snapshots from CRM simulations used for demonstrative purposes throughout the present paper. Section 3 introduces the mode decomposition method, and examines associated mathematical requirements. Particularly emphasized is the importance of the admissibility condition (see Eqs. (3.13) and (3.14) below) in order to make a mode decomposition mathematically well-posed. Section 4 shows how a general description of mode decomposition reduces to the mass-flux formulation, and discusses associated problems with this formulation. Section 5 examines wavelet decomposition as an alternative possibility. The wavelet has already been proposed by Yano *et al.* (2001a,b, 2004b: Y01a, Y01b, Y04b hereinafter) for analysing the CRM-simulated convective systems. The paper closes by summarizing the advantages and disadvantages of the two approaches in section 6.

2. CRM DATA SET

Three snapshots from CRM experiments are used in the present paper. Among those three, the first two snapshots are reviewed in the present section, because they are used throughout the paper. The last snapshot is used only in section 5(g), where further details are given.

These first two snapshots are from three-dimensional simulations. The first is 30 hours after the integration of a TOGA–COARE (Tropical Ocean Global Atmosphere Coupled Ocean–Atmosphere Response Experiment) period, starting from 1200 UTC 10 December 1992 (cf. Guichard *et al.* 2000). This corresponds to a weak-shear case, producing a nonsquall-type organized convective system (Fig. 1(a)). The second is from an ARM (Atmospheric Radiation Measurement experiment) period over the US Great Plains, starting from 1200 UTC 29 June 1997 (cf. Xu and Randall 2000; Xie *et al.* 2002; Xu *et al.* 2002). A snapshot corresponding to hour 15 of the integration is used here, which corresponds to a well-organized squall-line system under a strong wind shear (Fig. 1(b)). Here, also shown for reference, are the cloud-type classifications (Fig. 2) for both cases, which are further discussed in section 4(f).

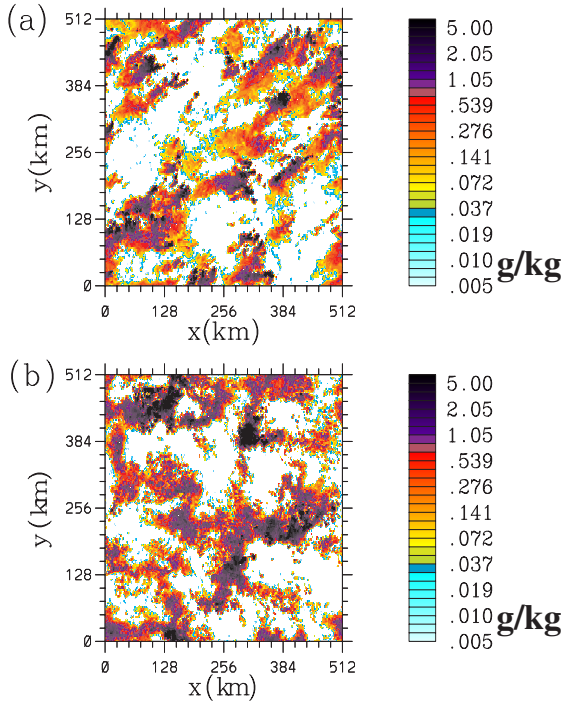

Figure 1. Top view of a snapshot from (a) the TOGA and (b) ARM case simulations. The total condensate (g kg^{-1}) at 5 km height is shown. The colour tones are given on a logarithmic scale.

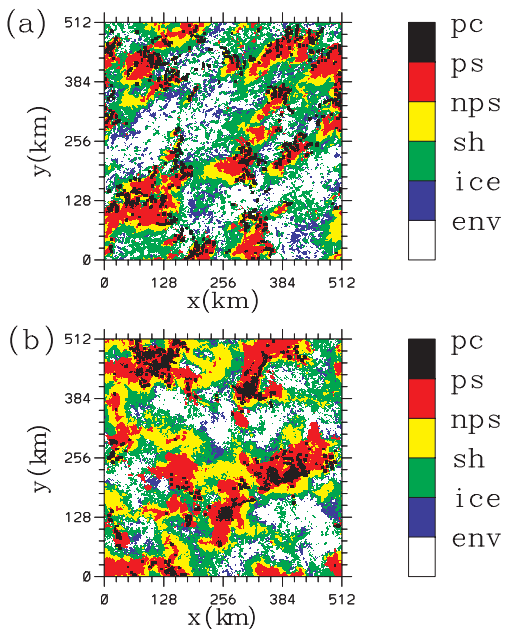

Figure 2. The cloud-type classification following Guichard *et al.* (1997). The classifications are made into precipitating convection (pc), precipitating stratiform (ps), non-precipitating stratiform (nps), shallow clouds (sh), ice anvils (ice), and the environment (env), as indicated by different colours. Snapshots from (a) the TOGA and (b) ARM case simulations are used as in Fig. 1.

Both experiments are performed with a non-hydrostatic anelastic mesoscale model (Meso-NH) jointly developed by the Laboratoire d'Aérologie and Centre National de Recherches Météorologiques/Groupe d'Étude de l'Atmosphère Météorologique (CNRM/GAME, cf. Lafore *et al.* 1998), with the model details referred to in the document on the Web (http://www.aero.obs-mip.fr/mesonh/). The model includes a 1.5-order turbulence scheme, a radiation scheme interacting with the clouds, and a prognostic bulk description of cloud physics. A doubly-periodic domain of size 512×512 km^2 with a horizontal resolution of 2 km is used. The model extends to 25 km with 47 vertical levels, given in fine resolution close to the surface (70 m at the lowest) and gradually stretched upwards to a cruder spacing of 0.7 km asymptotically. A sponge layer is placed above the 20 km level, and only the lowest 18 km are considered in the following. The model is relaxed towards observed domain-mean 'large-scale' winds, and is forced by 'large-scale' tendencies of temperature and moisture, a standard procedure for mesoscale CRM experiments (cf. Grabowski *et al.* 1996). The surface fluxes are prescribed in the ARM case, while the sea surface temperature is as in the TOGA–COARE case.

3. Mode decompositional problem

(*a*) *Subgrid-scale physical representation*

The prognostic equation for a physical variable φ (including the velocity $\mathbf{v}$) is typically expressed in dynamic meteorology as

$$\frac{\partial}{\partial t}\varphi = -\frac{1}{\rho}\nabla \cdot (\rho \mathbf{v}\varphi) + F, \tag{3.1}$$

where $\rho(z)$ is the reference density, which is assumed to be a function of height z only, and the last term F represents all the other physical processes that control the variable φ (the 'source' term hereinafter).

The source term is given by $F = Q_{\mathrm{R}} + L(c - e)$ and $F = e - c$, for example, for the dry static energy and the moisture mixing ratio, respectively, according to Arakawa and Schubert (see their Eqs. (14)–(17); also refer to Eqs. (4.2), (4.3) of Yanai and Johnson 1993). Here, Q_{R} is the radiative heating rate, c the water condensation rate, e the evaporation rate, and L the latent heat. Arakawa and Schubert's mass-flux formulation is reconstructed in section 4 under this more general prognostic equation (3.1). Thus, by choosing an appropriate set of variables for φ, Eq. (3.1) represents a *full* physical system for the subgrid-scale processes such as a CRM.

The resolution of a global model is limited to a finite scale, so the model can describe the system only in terms of the grid-box means. Thus, the above prognostic equation reduces to

$$\frac{\partial}{\partial t}\overline{\varphi} + \frac{1}{\rho}\overline{\nabla} \cdot (\rho \overline{\mathbf{v}}\,\overline{\varphi}) = -\frac{1}{\rho}\overline{\nabla \cdot (\rho \mathbf{v}'\varphi')} + \overline{F} \tag{3.2}$$

in a global model, where the overbar designates the horizontal mean over the grid box, the prime indicates the deviation from this mean (i.e. $\varphi' = \varphi - \overline{\varphi}$), and $\overline{\nabla}$ reminds that this nabla operation is performed over the global-model grid points. In this derivation, we have assumed that the nabla operator ∇ is interchangeable with the averaging operator, thus e.g., $\overline{\nabla\overline{\varphi}} = \overline{\nabla}\overline{\varphi}$. The goal of the subgrid-scale physical parametrization is to find a simple closed formulation for the right-hand side of Eq. (3.2).

(*b*) *Mode decomposition*

The basic idea of the mode decomposition approach resides in decomposing a physical variable, say $\varphi(x)$, defined in a one-dimensional space x of a range $[0, L]$ by a set of functions, say $\chi_l(x)$, that are characterized by an index l, i.e.

$$\varphi(x) \simeq \sum_{l=1}^{N} \widetilde{\varphi}_l \chi_l(x). \tag{3.3}$$

Here, $\widetilde{\varphi}_l$ is the coefficient of the lth mode defined under a certain normalization (see Eq. (3.4) below), and N modes are used for the above decomposition. Note that the above decomposition is not necessarily exact, but expected to approach exactness with increasing N.

The decomposition is facilitated when the above set of modes $\chi_l(x)$ satisfies an orthogonality given by

$$\frac{1}{L}\int_0^L \chi_l(x)\chi_m(x)\,\mathrm{d}x = \sigma_l \delta_{l,m} \tag{3.4}$$

with a normalization constant σ_l. Here, $\delta_{l,m}$ is Kronecker's delta. In that case, the coefficient of each mode is estimated by a simple projection of the mode onto a variable by the integral:

$$\widetilde{\varphi}_l = \frac{1}{\sigma_l L}\int_0^L \varphi(x)\chi_l(x)\,\mathrm{d}x. \tag{3.5}$$

A generalization of the above description of a variable $\varphi(x, y, z)$ in a three-dimensional space (x, y, z) is not unique. For the present purpose, the decomposition is performed with a set of modes $\chi_l(x, y)$ for horizontal patterns, so that

$$\varphi(x, y, z) = \sum_{l=1}^{N} \widetilde{\varphi}_l(z)\chi_l(x, y). \tag{3.6}$$

As a result, $\widetilde{\varphi}_l(z)$ defines the vertical profile of a mode. Here, we redefine Eqs. (3.4)–(3.5) by replacing the integrals with those over the two-dimensional domain defined by the coordinates (x, y). This fact is used in deriving the following results, especially Eq. (3.9).

Fourier decomposition is the best known example of mode decomposition. However, in order to make it effective, the set of modes $\chi_l(x, y)$ chosen must closely follow the characteristics of spatial distributions of the variables in the physical system of concern. Atmospheric convective systems often consist of various spatially isolated coherent structures, such as convective towers and stratiform clouds, hence a spatially well-isolated basic set is desirable.

Both the mass-flux decomposition and wavelets, considered specifically in the following two sections, satisfy this requirement. Note that the mass-flux decomposition is a special case that reduces to a partitioning of the 'grid-box' domain into subregions. On the other hand, mode decomposition generally allows an overlapping of modes.

(*c*) *Prognostic representation of the subgrid-scale processes*

Under an orthogonal mode expansion satisfying Eq. (3.4), the system (3.1) is transformed into a description in terms of the mode coefficients $\widetilde{\varphi}_l$ by multiplying Eq. (3.1) with the mode χ_l and integrating over the horizontal 'grid-box' domain:

$$\frac{\partial}{\partial t}\widetilde{\varphi}_l = -\widetilde{(\nabla_{\mathrm{H}} \cdot \mathbf{v}_{\mathrm{H}}\varphi)_l} - \frac{1}{\rho}\frac{\partial}{\partial z}\rho\widetilde{(w\varphi)}_l + \widetilde{F}_l, \tag{3.7}$$

where the horizontal and vertical flux terms are given by

$$\widetilde{(\nabla_{\mathrm{H}} \cdot \mathbf{v}_{\mathrm{H}}\varphi)}_l = \sum_{j,k} (a_{j,k,l}\widetilde{u}_j + b_{j,k,l}\widetilde{v}_j)\widetilde{\varphi}_k, \tag{3.8a}$$

$$\widetilde{(w\varphi)}_l = \sum_{j,k} c_{j,k,l}\widetilde{w}_j\widetilde{\varphi}_k \tag{3.8b}$$

with the coefficients $a_{j,k,l}$, $b_{j,k,l}$, and $c_{j,k,l}$ defined from the orthogonality of the modes as

$$a_{j,k,l} = \frac{1}{L_x L_y \sigma_l} \int_0^{L_y}\int_0^{L_x} \frac{\partial(\chi_j\chi_k)}{\partial x}\chi_l \,\mathrm{d}x\,\mathrm{d}y \tag{3.9a}$$

$$b_{j,k,l} = \frac{1}{L_x L_y \sigma_l} \int_0^{L_y}\int_0^{L_x} \frac{\partial(\chi_j\chi_k)}{\partial y}\chi_l \,\mathrm{d}x\,\mathrm{d}y \tag{3.9b}$$

$$c_{j,k,l} = \frac{1}{L_x L_y \sigma_l} \int_0^{L_y}\int_0^{L_x} \chi_j\chi_k\chi_l \,\mathrm{d}x\,\mathrm{d}y \tag{3.9c}$$

for a horizontal 'grid-box' domain $L_x \times L_y$.

The derived set of equations, systems ((3.7)–(3.9)), constitutes a full *prognostic* description of the original physical system (3.1) over the 'grid-box' domain under mode decomposition. Its severe truncation serves as a subgrid-scale representation for global models, when selected modes approximate the full system closely. The mass-flux formulation is a special example derived under this framework, and the formulation presented here provides its generalization.

This formulation is also general in the sense that all the physical processes associated with the source F considered in the original CRM system are also included. Note that not all of these physical processes are necessarily included in current cumulus parametrizations. Thus, this methodology provides a framework for a unified subgrid-scale physical representation.

In time-integrating the system (3.7), evaluations of all the terms are straightforward with given expansion coefficients φ_l, except for the source term $\widetilde{F}_l$. This last term requires special consideration, and is discussed separately in sections 4(g) and 5(c) for the two decomposition methods. Conversely, the quantities in Eqs. (3.7)–(3.9) can be directly diagnosed from CRM data, once a decomposition (3.6) is established. Thus, any specific subgrid-scale parametrization developed from this prognostic representation (3.7) can be directly and systematically verified by CRM data, including the closure hypotheses. In this way, the mode decomposition approach permits a systematic verification of a developed parametrization from CRM.

(*d*) *Domain-mean contributions*

The system (3.7) constitutes a subgrid-scale representation, because it provides the evaluation of domain-mean contributions that are required in the right-hand side of Eq. (3.2). The vertical fluxes are evaluated with a help of the Parseval formula (cf. Mallat 1998, section 2.2.2), when the orthogonality (3.4) is satisfied, by

$$\overline{w\varphi}(z) = \sum_{l=1}^{N} \sigma_l \widetilde{w}_l(z)\widetilde{\varphi}_l(z), \tag{3.10}$$

where the vertical velocity w is also expanded in an analogous manner to φ. Horizontal fluxes are also evaluated similarly.

Additionally, the 'grid-box' domain-mean of source F (the second term) is evaluated by

$$\overline{F(z)} = \sum_{l=1}^{N} \widetilde{F}_l(z)\overline{\chi_l(x,\, y)}. \tag{3.11}$$

Thus, the total domain-mean source is given by a sum of contributions from various subcomponents, such as convective and stratiform components (Houze and Betts 1981; Houze 1989; Rutledge 1991; Moncrieff 1995). Such a decomposition is possible only if modes have non-vanishing contributions to the domain mean, i.e.

$$\overline{\chi_l(x,\, y)} \neq 0. \tag{3.12}$$

This is a first condition required in order to apply the mode decomposition to the subgrid-scale physical representation. Physically it is *desirable* to decompose the domain-mean source into various modes, although mathematically it is sufficient to have only one mode that satisfies this condition.

(*e*) *Admissibility*

Note that once a set of modes $\chi_l(x)$ that satisfies the orthogonality (3.4) is chosen, it is straightforward to transform the original full system (3.1) into the mode-decomposition based description (3.7). However, it is harder to find such a set of modes that can approximate the full physical field by Eq. (3.3) or (3.6). The ability of the mode set that recovers the original function $\varphi(x)$ by sum (3.3) or (3.6) is called the *completeness* mathematically. This concept may be slightly generalized as a *reconstruction*, when the decomposition is redundant (i.e. overcomplete), hence weighting may be applied (cf. Mallat, chapter 4) in the above mode expansion (3.3). Obviously the choice of mode sets is not arbitrary in order to be *reconstructable*, but must satisfy a certain mathematical condition, as presented for a one-dimensional case here.

Recall that atmospheric convective systems are more than often characterized by spatially isolated modes, so that in small-scale limits, they may be represented by a translation x_0 and a rescaling s of an isolated shape of the prototype, say $\chi(x)$, so that we may consider a set of modes $\chi((x - x_0)/s)$ characterized by these two parameters x_0 and s. Note that both the mass-flux and the wavelet decompositions satisfy this property. Especially, $\chi(x)$ corresponds to the mother wavelet in the wavelet decomposition (cf. section 5(a)). By focusing on those small-scale limits, we may take the limit of infinite domain, i.e. $L \to \infty$, for simplicity. Under this framework, a theorem can be derived (see e.g. Mallat 1998, section 4.3.1 for the proof), which shows that a sufficient condition for this set to be *reconstructable* is to satisfy

$$\int_0^\infty \frac{|\hat{\chi}(k)|^2}{k}\, \mathrm{d}k < \infty, \tag{3.13}$$

which is called the admissibility condition, where $\hat{\chi}(k)$ is the Fourier transform of $\chi(x)$. A direct consequence of this constraint is $\hat{\chi}(0) = 0$ (because otherwise the integral above may become singular), hence the domain mean must vanish, i.e.

$$\overline{\chi_l(x)} = 0 \tag{3.14}$$

for all the modes with $l = 1, \ldots, N$.

This is the second important condition for the mode decomposition; unfortunately, in direct contradiction to the first, (3.12). The discrete wavelet considered in section 5

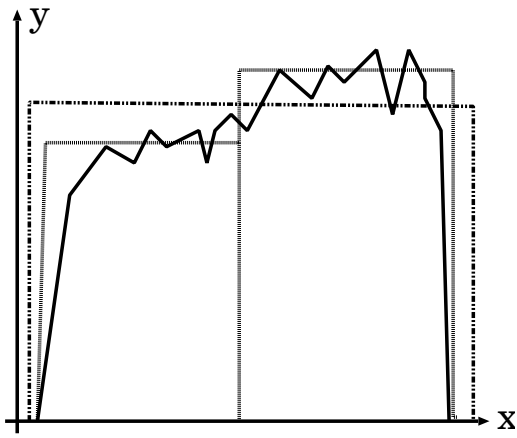

Figure 3. Schematics for illustrating an arbitrariness of the segmentally constant approximation. See the text for details.

is constructed to satisfy this admissibility condition (3.14), hence all the modes have vanishing domain-mean value except for the domain-mean mode which is simply a constant.

More generally, under the multiresolution analysis (see e.g. Mallat 1998, chapter 7 for more details), the wavelet expansion for increasing scales can be terminated at a certain scale, and above this scale it is replaced by a set of so-called scaling functions, which characterize the structure at this termination scale, with non-vanishing domain-mean values. Note that this termination scale can be chosen arbitrarily. Therefore, an approximate mode decomposition with non-vanishing domain-mean values (cf. Eq. (3.12)) is always possible when a scale of interests is fixed (thus s is fixed in the above), for example to the mesoscale.

However, the admissibility condition (3.14) implies that a decomposition over multiple scales such as over both convective and meso-scales is no longer possible in a unique manner. Generally speaking, when a decomposition of domain-mean quantities is intended by satisfying the condition (3.12), a unique decomposition becomes no longer possible.

For example, imagine an updraught region is shown by the solid curve in Fig. 3. The simplest square-pulse approximation is to fit this updraught region with a single square pulse (double-chain dashed), but it is also tempting enough to fit it with two square pulses (short-dashed), because the updraught tends to be stronger to the right-hand side. It follows that it is not obvious how to limit the number of pulses in order to *reasonably* approximate a given updraught. More pulse modes can more accurately represent this updraught, but a lower number of modes is always desirable for efficiency of representation. How to make a compromise between these two requirements is not always obvious, and depends on the criterion posed.

(*f*) *Physically-defined subcomponents*

Finally, more physically-defined subcomponents (e.g. cloud types) may be introduced as subsets of the above decomposition, say

$$\sum_{j=1}^{J_k} \widetilde{\varphi}_{l_j,k}(z)\chi_{l_j}(x, y) \tag{3.15}$$

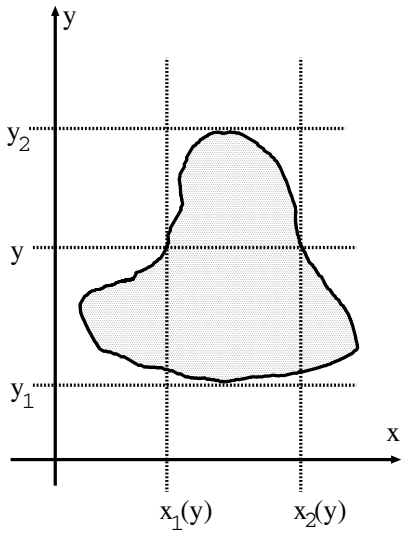

Figure 4. The definition of the square-pulse region (shaded grey) by the two boundary points $\mathbf{r}_1 = (x_1, y_1)$, and $\mathbf{r}_2 = (x_2, y_2)$. Here, $(x_1(y), x_2(y))$ marks the left and the right edges of the region defined for the range $y_1 \leqslant y \leqslant y_2$. Within this grey region, $\mathcal{M}(\mathbf{r}_\mathrm{H}|\mathbf{r}_1, \mathbf{r}_2) = 1$, otherwise $\mathcal{M}(\mathbf{r}_\mathrm{H}|\mathbf{r}_1, \mathbf{r}_2) = 0$.

for a kth mode, which is defined by J_k modes with expansion coefficients $\widetilde{\varphi}_{l_j,k}(z)$. These physical subcomponents may correspond to different cloud types such as convective towers and stratiform clouds. The effective number of modes can further be reduced by binding the modes together into these subcomponents. Equation (3.15) may be considered as a generalization of the spectrum model introduced by Arakawa and Schubert (1974): (see section 4(a) below).

4. Mass-flux based decomposition

A mass-flux based mode decomposition is discussed in section 4(a), then the auxiliary conditions required for the construction of the mass-flux formulation in section 4(b). A detailed overview of the mass-flux formulation is provided in sections 4(c) and 4(d) under this mode-decomposition framework. Advantages and disadvantages of this approach are discussed in the remainder of the section.

(*a*) *Expansion basis of the mass-flux formulation*

The main idea of the mass-flux formulation (cf. Yanai *et al.* 1973; Arakawa and Schubert 1974) *may* be considered as that of dividing the horizontal 'grid-box' domain into a set of subdomains that individually have constant physical values over a horizontal cross-section (cf. Fig. 2 of Yanai *et al.*: segmentally constant decomposition). Thus, physical variables are decomposed into a set of square-shaped pulses, defined for example by $\mathcal{M}(\mathbf{r}_\mathrm{H}|\mathbf{r}_1, \mathbf{r}_2)$ with $\mathbf{r}_\mathrm{H} = (x, y)$, $\mathbf{r}_1 = (x_1, y_1)$, and $\mathbf{r}_2 = (x_2, y_2)$, where $(x_1(y), x_2(y))$ is the range of the square pulse in the x-direction defined as a function of y for the range (y_1, y_2) (Fig. 4)†. Within this square-pulse region, this function takes the value one, otherwise 0. In a one-dimensional system, we simply designate it by $\mathcal{M}(x|x_1, x_2)$ with the pulse region defined by (x_1, x_2).

† The role of x and y here are, of course, interchangeable.

As a result, a variable, $\varphi(x, y, z)$, over this horizontal domain may be approximated by N square-pulses by setting $\chi_l(x, y) = \mathcal{M}(\mathbf{r}_\mathrm{H}|\mathbf{r}_1^l, \mathbf{r}_2^l)$ in Eq. (3.6), where the index l characterizes the boundary vectors $\mathbf{r}_1^l$, $\mathbf{r}_2^l$. It is especially designed to perform a decomposition of the domain-mean quantities (cf. Eq. (3.11)) by satisfying the condition (3.12) with the domain mean $\overline{\mathcal{M}(\mathbf{r}_\mathrm{H}|\mathbf{r}_1^l, \mathbf{r}_2^l)} = \sigma_l$ corresponding to the fractional area occupied by the lth mode. Furthermore, by assuming that $\mathcal{M}(\mathbf{r}_\mathrm{H}|\mathbf{r}_1^l, \mathbf{r}_2^l)$ $(l = 1, \ldots, N)$ are not overlapping each other, the orthogonality (3.4) is guaranteed.

In developing the standard mass-flux formulation (Yanai *et al.* 1973; Arakawa and Schubert 1974), these segmentally constant subdomains are further classified into the physical subcomponents, as defined by Eq. (3.15). Within these subcomponents, we assume that all the modes share the same vertical profile. These physical subcomponents may occupy several non-overlapping areas. These segmentally constant subcomponents are further categorized into two major classes: 1) a single mode (environment: with the subscript 'env' in the following) representing a characteristic state of non-convective environment, 2) the remaining convective components associated with both updraughts and downdraughts.

(*b*) *Auxiliary conditions*

In order to fulfil requirements for the standard mass-flux formulation (Yanai *et al.* 1973; Arakawa and Schubert 1974), three *auxiliary* conditions are posed on the segmentally constant decomposition:

(1) Generally, these square-pulse modes must be vertically aligned, although their areas may change with height. The simplest way to satisfy this requirement is to assume that the horizontal distribution of the square pulses is identical at every vertical level. In other words, the boundaries $[\mathbf{r}_1^j, \mathbf{r}_2^j]$ $(j = 1, \ldots, N)$ of these segmentally constant subdomains are height independent, as already implied in Eq. (3.6).

(2) Identical distributions of the subcomponents are assumed for all physical variables. In other words, the boundaries $[\mathbf{r}_1^j, \mathbf{r}_2^j]$ are common to all variables.

(3) The convective draught subcomponents defined above are always directly adjacent to the environment, so that the lateral exchanges of the air masses through the boundaries are restricted to those between the environment and the individual draughts. As a result, the other types of nonlinear interaction between the modes are excluded.

We call it the *mass-flux decomposition* when these auxiliary conditions are satisfied for a segmentally constant decomposition.

(*c*) *The mass-flux based representation*

The prognostic equation for the mass-flux decomposed system is derived in an analogous manner as for Eq. (3.7). Thus, we multiply $\sum_{j=1}^{J_k} \mathcal{M}(\mathbf{r}_\mathrm{H}|\mathbf{r}_1^{k,j}, \mathbf{r}_2^{k,j})$ with Eq. (3.1) and integrate it over the whole domain, which leads for each draught component ($k \neq$ env) to

$$\frac{\partial \widetilde{\varphi}_k(z)}{\partial t} = -\frac{1}{\rho(z)}\frac{\partial}{\partial z}\rho(z)\widetilde{w}_k(z)\widetilde{\varphi}_k(z) + \frac{\lambda_k(z)}{\sigma_k}\widetilde{\varphi}_k^*(z) + \widetilde{F}_k, \tag{4.1}$$

where λ_k is the lateral exchange rate of the air with the environment, and $\widetilde{\varphi}^*_k(z)$ is the value of the mode at the boundary with the environment. The former is given by

$$\begin{aligned}\lambda_k &= -\frac{1}{L_x L_y}\sum_{j=1}^{J_k}\oint_{\partial S_{k,j}} \mathbf{v}_{\mathrm{H}}\cdot \mathrm{d}\mathbf{r} \\ &= \frac{\sigma_k}{\rho}\left(\frac{\partial \rho \widetilde{w}_k}{\partial z}\right). \end{aligned} \tag{4.2}$$

The line integral above is performed over the boundary $(\mathbf{r}_1^{k,l}, \mathbf{r}_2^{k,l})$ designated by $\partial S_{k,j}$. The last expression is obtained from the mass continuity. For the boundary values, one usually takes the upstream approximation, hence the draught value $\widetilde{\varphi}^*_k(z) = \widetilde{\varphi}_k(z)$ when detraining ($\lambda_k(z) < 0$), and the environmental value $\widetilde{\varphi}^*_k(z) = \widetilde{\varphi}_{\mathrm{env}}(z)$ when entraining ($\lambda_k(z) > 0$). Also, the fractional area σ_k occupied by the kth subcomponent is assumed constant with time (cf. Gregory and Miller 1989).

The standard approximation further assumes that the total convective area is much smaller than the total domain, i.e. $\sum_{k\neq \mathrm{env}} \sigma_k \ll 1$. As a result, the 'grid-box' domain-averaged tendency of a variable can be approximated by that of the environment. The latter is simply obtained in an analogous manner as for individual draught components, but with the lateral exchanges (detrainment–entrainment) given in terms of a sum of contributions from all the draught components:

$$\begin{aligned}\frac{\partial \overline{\varphi}(z)}{\partial t} \simeq \frac{\partial \widetilde{\varphi}_{\mathrm{env}}(z)}{\partial t} &= -\frac{1}{\rho(z)}\frac{\partial}{\partial z}\rho(z)\widetilde{w}_{\mathrm{env}}(z)\widetilde{\varphi}_{\mathrm{env}}(z) \\ &\quad - \sum_{k\neq \mathrm{env}} \lambda_k(z)\widetilde{\varphi}^*_k(z) - \overline{\nabla}\cdot\overline{\mathbf{v}}\overline{\varphi} + \widetilde{F}_{\mathrm{env}}. \end{aligned} \tag{4.3}$$

The third term from the last is obtained by using the balance of lateral exchanges:

$$\lambda_{\mathrm{env}}(z)\widetilde{\varphi}^*_{\mathrm{env}}(z) = -\sum_{k\neq \mathrm{env}} \lambda_k(z)\widetilde{\varphi}^*_k(z),$$

whereas the second from the last arises from the additional exchange over the lateral boundary of the 'grid box' domain.

Equation (4.1) is equivalent to Eqs. (43)–(50) of Arakawa and Schubert (1974), corresponding to their budgets for mass, static energy, water vapour and liquid water. Equation (4.3) is equivalent to Eqs. (29) and (30) of Arakawa and Schubert (1974)†, and Eq. (4) of Bechtold *et al.* (2001), for example. Thus, in this manner, the mass-flux formulation can be derived directly from a more general framework of mode decompositions as discussed in section 3.

(*d*) *Mass-flux based convective parametrizations*

The standard mass-flux based convective parametrizations proposed by Arakawa and Schubert (1974) and followed in many subsequent works (e.g. Bougeault 1985; Tiedtke 1989; Gregory and Rowntree 1990; Bechtold *et al.* 2001) are based on further reductions of the prognostic equation (4.1).

† As a major difference, the latter is given in terms of an advection form in contrast to the flux form here.

The evolution of the total convective field $\sum_{k\neq\mathrm{env}} \sigma_k \widetilde{\varphi}_k$ is given by taking a sum of Eq. (4.1) after weighting with σ_k:

$$\frac{\partial}{\partial t}\sum_{k\neq\mathrm{env}} \sigma_k \widetilde{\varphi}_k(z) = -\frac{1}{\rho(z)}\frac{\partial}{\partial z}\sum_{k\neq\mathrm{env}} \rho(z)\sigma_k \widetilde{w}_k(z)\widetilde{\varphi}_k(z) + \sum_{k\neq\mathrm{env}} \lambda_k(z)\widetilde{\varphi}^*_k(z) + \sum_{k\neq\mathrm{env}} \sigma_k \widetilde{F}_k. \tag{4.4}$$

Again, if $\sum_{k\neq\mathrm{env}} \sigma_k \ll 1$, the left-hand side of Eq. (4.4) becomes much smaller than individual terms in the right-hand side, by also assuming that the degree of the variations of the physical variables (including the mass flux $\sigma_k \widetilde{w}_k$ but not the vertical velocity $\widetilde{w}_k$ itself) within convective draughts is of the same order of magnitude as that for the domain-mean variables. Then, a steady state can be assumed for Eq. (4.4), hence it reduces to a diagnostic relation. These diagnostic relations are used to obtain the closed expressions for source due to the cloud physical processes (primarily, condensation c and evaporation e) in terms of the draught values $\widetilde{\varphi}_k(z)$ and the mass fluxes $\rho\widetilde{w}_k(z)$. The draught values $\widetilde{\varphi}_k(z)$ are commonly estimated by moist adiabatic ascent and descent of an air parcel, but also include lateral mixing effects (detrainments and entrainments). Thus, the whole problem reduces to that of defining the convective mass fluxes.

In standard procedures, vertical profiles of these mass fluxes are fixed either as a spectrum (Arakawa and Schubert 1974) or a single mode (bulk mass-flux). In either case, the problem reduces to that of defining the mass fluxes at the cloud base. This constitutes the so-called closure problem, where various hypotheses (cf. Arakawa and Schubert 1974; Kuo 1974) are introduced.

(*e*) *Lack of admissibility*

Thus, in this manner, we have arrived at a starting point (Eqs. (4.1) and (4.3)) for the mass-flux formulation by a mode decomposition approach. The bulk of the work for developing a mass-flux based parametrization resides in what follows from here, as outlined in the previous subsection. Although these issues are beyond the scope of the present paper, it is emphasized here that these subsequent reductions from Eqs. (4.1) and (4.3) *could* be in principle directly verified from CRM data under the mode decomposition framework, if a mass-flux decomposition *were* performed on CRM data.

This is exactly where the main disadvantage of the mass-flux formulation resides. Due to the lack of admissibility (3.14), the segmentally constant decomposition cannot be performed in a unique manner. The choice of a set of modes for $\{\mathbf{r}^j_1, \mathbf{r}^j_2\}$ that satisfies Eq. (3.6) becomes non-trivial under any approximations, as schematically demonstrated by Fig. 3 above. For this reason, the *formal* application of the mass-flux decomposition on CRM data is not practical, and is hardly ever attempted.

(*f*) *Cloud-type classification: practical procedure*

In place of this formal mode decomposition approach, a much simpler procedure is generally taken, in which the CRM grid-columns are classified by cloud type. This method, originally developed in radar data analysis (Houze 1977) for cloud-type classifications, is widely used in analysing atmospheric convective systems both in modelling (Tao and Simpson 1989; Sui *et al.* 1994; Xu 1995) and observations (Churchill and Houze 1984; Steiner *et al.* 1995). Some studies also use simpler classifications based

on the *local* vertical velocity (e.g. Gregory and Miller 1989) amounting to a pointwise classification.

In the CRM applications, the obtained cloud types are further used as substitutes for the piecewise-constant modes, $\widetilde{\varphi}_k(z)\sum_{j=1}^{J_k}\mathcal{M}(\mathbf{r}_{\mathrm{H}}|\mathbf{r}_1^{k,j},\mathbf{r}_2^{k,j})$, as defined in section 3(f), by applying the approximations

$$\widetilde{w}_k(z) \simeq \overline{w}_k(z) \tag{4.5a}$$

$$\widetilde{\varphi}_k(z) \simeq \overline{\varphi}_k(z), \tag{4.5b}$$

where $\overline{(\ )}_k$ designates a mean over the kth cloud type.

As an example of such a cloud-type classification, we adopt the one developed by Guichard *et al.* (1997) with a minor change of threshold values introduced by Yano *et al.* (2004a), in which six cloud types are considered: (1) precipitating convection (pc), (2) precipitating stratiform (ps), (3) non-precipitating stratiform (nps), (4) shallow clouds (sh), (5) ice anvils (ice), and (6) the clear sky area ('environment': env).

The resulting classification (Fig. 2, see above) appears to be reasonable as far as it is interpreted as a map of cloud types, as indicated by the distribution of the total condensate in Fig. 1. The cloud-type classification is also well suited for the decompositional analysis for the domain-mean values defined by Eq. (3.11). However, the classification map already visually demonstrates a difficulty of performing a mass-flux decomposition by satisfying the third auxiliary condition (section 4(b)): precipitating convection is surrounded by precipitating stratiform clouds everywhere.

This classification is also not constrained by the segmentally constant approximation to any degree, although such an approximation (i.e. Eq. (4.5)) may be introduced a posteriori. The obtained decomposed fields are far from homogeneous, retaining the same degree of variability as the total field (cf. Fig. 1). The probability distribution of a variable inside a given cloud type remains overall the same as that of the total (cf. Figs. 3 and 4 of Yano *et al.* 2004a), which is far from Dirac's delta (top-hat distribution, as commonly called). As an obvious consequence, a direct application of Eq. (3.10) to the cloud-type classification substantially underestimates the vertical fluxes (cf. Guichard *et al.* 1997; Yano *et al.* 2004a). Although a further increase of the number of 'cloud types' may lead to a more accurate statistical description of the convective system (cf. Yano *et al.* 2004a), it is unlikely to satisfy the auxiliary conditions (cf. section 4(b)) for the mass-flux decomposition.

(*g*) *Source evaluation*

A common practice for evaluating the domain-mean source term $\overline{F}$ in Eq. (3.2) is to separate it into those parts due to the grid-box mean variables $\overline{F}^* \equiv F(\overline{\varphi},\dots)$ and a remaining part $F'^* = \overline{F} - \overline{F}^*$, and attempt to parametrize the latter part (i.e. subgrid-scale source) independent of the former (i.e. large-scale source). Especially, when the limit $\sum_{k\neq\mathrm{env}}\sigma_k \to 0$ is taken under the mass-flux formulation, the environmental contribution becomes equal to the large-scale source, i.e. $\overline{F}^* = \widetilde{F}_{\mathrm{env}}$, and $F'^* = \sum_{k\neq\mathrm{env}}\sigma_k\widetilde{F}_k$. These two terms can readily be evaluated, because the real space values at local points are directly represented by the mass-flux mode values. However, the separation principle, $\overline{F} = \overline{F}^* + F'^*$, does not work in general unless a homogeneous environmental mode that occupies a majority part of the 'grid-box' domain can be defined. Thus, generally, the evaluation of F'^* becomes non-trivial due to the strong nonlinearities in the source term.

5. WAVELET-BASED APPROACH

With earlier contributions (Y01a,b, Y04b) in mind, the present section succinctly lists pertinent points in applying the wavelet for developing and verifying subgrid-scale physical representations. Section 5(g) presents a very preliminary result towards such developments. The last subsection, 5(h), makes a little detour in order to re-address the mass-flux decomposition problem from a wavelet point of view.

(*a*) *Basics*

As is the case for mass-flux decomposition, the wavelets are designed to represent spatially isolated structures efficiently. A discrete set for the parameters x_0 and s introduced in section 3(e) is chosen in such a way that the set satisfies completeness (cf. Fig. 4 of Y01a). Designating the wavelets by $\psi_l(x)$, the wavelet decomposition is recovered by setting $\chi_l(x) = \psi_l(x)$ and $\chi_l(x, y) = \psi_{l_x}(x)\psi_{l_y}(y)$ for one- and two-dimensional cases in section 3 with l_x and l_y the wavelet indices for x- and y-directions, respectively.

(*b*) *Compressed representation*

The main advantage of using wavelets is in their capacity to efficiently represent spatially isolated coherent features common in atmospheric convective systems (Y01a,b, Y04b). This is achieved: (1) by taking spatially isolated modes, as in the case of the segmentally constant decomposition, and (2) by taking a complete orthogonal set. According to Y04b, the overall reduction of the system variability remains 10–20% when only 10% of the total number of modes is retained. A further compression of the system is feasible when a 'renormalization' is taken (Yano *et al.* 2003).

(*c*) *Prognostic description*

The deduction from the originally full system (3.1) to the reduced form (3.7) is straightforward: the decomposition can be directly performed by Eq. (3.4) by adopting a complete, orthogonal set. A high truncation can be applied to the resulting *prognostic* representation (3.7) due to a high compressibility of the wavelet decomposition.

On the other hand, the source $\widetilde{F_k}$ in Eq. (4.1) is not readily evaluated in wavelet space due to an overlapping of wavelet modes. Instead, it must be evaluated directly in real space after inverse wavelet transform, in an analogous procedure to the transformed-Fourier approach. Nevertheless, even for this procedure, we may take advantage of high compressibility by limiting the number of spatial points to an equivalent level.

(*d*) *Role of domain-mean: eddy–eddy interactions*

A major practical drawback with the wavelets may be that we cannot decompose the domain-mean values (e.g. total precipitation) into subcomponents (e.g. convective and mesoscale contributions), because the domain-mean value is simply dealt with as a single independent mode by satisfying the admissibility condition (cf. section 3(e)). However, this is not a fundamental flaw in any sense for constructing a subgrid-scale representation. It is rather consistent with a standard description in terms of eddy–eddy interactions in turbulence studies as well as in middle atmosphere dynamics (cf. Andrews and McIntyre 1978a,b,c).

(*e*) *Choice of wavelets*

Among wide ranges of complete orthogonal wavelet sets available, we suggest using analytically smooth wavelets such as Meyer, as adopted in section 5(g), because the analytical smoothness enables the fitting of spatially isolated physical features efficiently (Y04b). A good localization in Fourier space furthermore guarantees a compact expression of nonlinearity in terms of the tensors $a_{j,k,l}$, $b_{j,k,l}$, $c_{j,k,l}$ (cf. Eqs. (3.9a, b, c)). However, in certain cases, it is also preferred to use a highly digitalized wavelet such as the Haar as adopted in section 5(h) below.

(*f*) *Decomposition into subcomponents*

As in the case with the segmentally constant decomposition, the wavelet can also categorize the *eddy component* of the system (but not the domain means, cf. section 5(d)) into various physically defined subcomponents under the general framework discussed in section 3(f). Such a specific procedure is proposed by Y01b (refer especially to their Fig. 1). Importantly, the resulting physical fields for these subcomponents are continuous spatially (cf. Figs. 3–5 of Y01b). After a decomposition into subcomponents, contributions of various quantities such as vertical eddy fluxes from these subcomponents can readily be evaluated. For example, a mass flux is computed in Y01b and compared with a result using a columnwise cloud-type classification.

(*g*) *Temporal development of convection in wavelet space*

By retaining the full nonlinearity in Eq. (3.7), the wavelet-based representation can consider *full nonlinear interactions between the modes in an efficient manner*, in contrast to the mass-flux decomposition, in which nonlinearity is inherently limited to those with the environment over the lateral boundaries.

Here, such a capacity of wavelets is indicated by a diagnostic analysis at a moment of triggering of convection in an idealized two-dimensional experiment of the diurnal cycle over a midlatitude continent reported in detail by Chaboureau *et al.* (2004; see also Yano *et al.* 2005). We specifically adopt a horizontally one-dimensional domain here in order to facilitate the graphic representation of wavelet modes. The horizontal domain size is $L_x = 512$ km and it extends vertically above 20 km. The horizontal resolution is 2 km, giving $N = 256$ points horizontally, with the vertical resolution similar to the other cases. Surface heat fluxes are prescribed in order to mimic an idealized diurnal cycle. The triggering mechanism of convection under the diurnal cycle of forcing is yet to be fully understood.

A triggering of convection is characterized by a conversion C of the available potential energy P into a vertical component K_{V} of the kinetic energy. The analysis of this conversion process in wavelet space quantifies where and at what scale the triggering occurs. These quantities P, C, K_{V} defined in wavelet space (see the appendix for details) are plotted in Fig. 5 at the moment of triggering (on day 3 at 12:48 local time) as integrals over the whole vertical domain. Clearly identified are both the horizontal localizations (horizontal axis) and scales (wavenumber k: vertical axis) of the modes that are critically contributing to the triggering of convection, by converting the potential energy Fig. 5(c) to the kinetic energy (a), as measured by energy conversion rate (b). The number of modes significantly contributing to this process is clearly limited, supporting the efficiency of the wavelet representation. The distributions of wavelet spectra for K_{V} and C are well correlated, indicating that this conversion process is responsible for the generation of K_{V}.

Due to the spatially isolated structure of wavelets, each dominant mode can be identified with corresponding spatially isolated structures in real space. In the above example, the three dominant modes for P at the smallest scale are identified with cold pools in the boundary layer, which are contributing to the triggering. Importantly, the methodology is applicable not only to the convective scales, but also to global phenomena such as Madden–Julian oscillations (Yano 2004). In the latter application, the nonlinear mode–mode interactions have also been evaluated.

(*h*) *Segmentally constant decomposition by Haar wavelets*

Finally, when the Haar wavelet is adopted in place of the Meyer, interestingly, a segmentally constant decomposition introduced in section 4(a) is achieved *approximately*, but without satisfying the auxiliary conditions of section 4(b). The mother wavelet for the Haar (see e.g. Fig. 1(b) of Y04b) is a pair of negative and positive square-shaped pulses such that

$$\chi(x) = -\mathcal{M}(x|-1/2, 0) + \mathcal{M}(x|0, 1/2),$$

where $\mathcal{M}(x_1, x_2)$ is a one-dimensional version of the square-pulse function introduced in section 4(a). Its complete set is constructed by the procedure outlined in section 5(a).

A single Haar wavelet constitutes a square-shaped updraught and downdraught couplet, as in the mass-flux formulation. With the aid of the Haar wavelet, a segmentally constant decomposition is achieved (Fig. 6) in which the system is compressed by retaining only 1% of leading modes in the Haar-wavelet expansion (corresponding to the threshold $\mu = 5$ in Eq. (2.7) of Y04b). Thus, the mass-flux based interpretations can be to some extent recovered under the Haar wavelet.

At the same time, this decomposition demonstrates an arbitrariness of the segmentally constant decomposition pedagogically. Here, all the subdomains are square-shaped, although these shapes could be chosen more freely. The auxiliary conditions imposed on the mass-flux representation (cf. section 4(b)) are also inherently difficult to satisfy. Distributions of the total water content and the vertical velocity are obviously not identical, against the second auxiliary condition. Defining a horizontally homogeneous region as an 'environment' (cf. section 4(g)) is not easy, nor is placing all the convective components directly adjacent to the environment (third auxiliary condition).

6. Conclusions

(*a*) *Overview*

Mode decomposition is proposed as a general methodology for directly verifying and developing convective-scale physical representations for global models by analysing convective systems simulated by a CRM. As specific examples, the mass flux and the wavelet are considered, but without excluding the possibilities of different types of mode sets that provide more efficient representations of the subgrid-scale processes.

Under mode decomposition, the full *prognostic* system (3.1) reduces to Eq. (3.7). A highly truncated version of Eq. (3.7) itself can be used as a prognostic representation of subgrid-scale processes for global models when the adopted mode decomposition is highly effective. The accuracy of this representation scheme can be verified directly from the CRM when the decomposition satisfies the admissibility, because then each term in Eq. (3.7) can be evaluated from the originally full system ((3.1), e.g. CRM).

The system (3.7) may further be reduced to a *parametrization* by introducing various approximations (such as instantaneous adjustments) and hypotheses (so-called closures). This reduction constitutes a large part of the difficulties in developing subgrid-scale parametrizations. An important emphasis of the present paper is that as long as

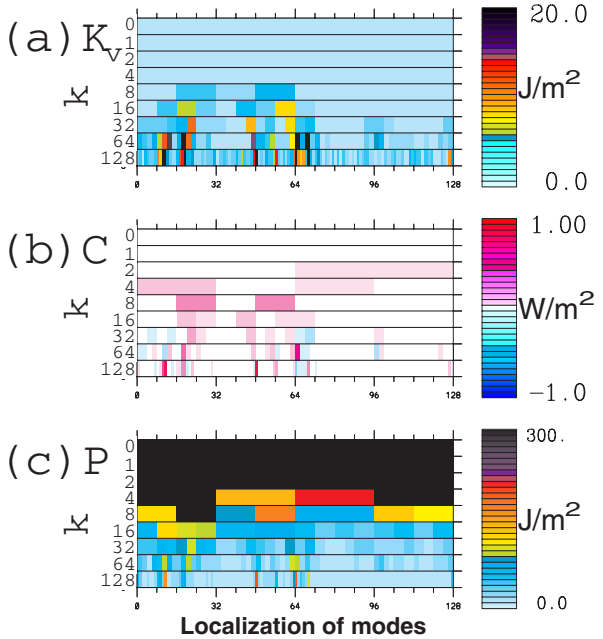

Figure 5. Energy cycle in the wavelet space at a moment of convective triggering under an idealized diurnal cycle: (a) the vertical component $\tilde{K}_{V,l}$ of the kinetic energy, (b) the conversion rate $\tilde{C}_l$, and (c) the available potential energy $\tilde{P}_l$ as defined by Eqs. (A.5), (A.6), and (A.4), respectively, in the appendix. The spatial localization of modes is indicated by the horizontal axis in the scale of the smallest wavelet modes, and their scales by the 'wave number' k increasing downwards in the vertical axis. The values of the wavelet coefficients are given by tones in a box at the corresponding localization and the 'wave number'. The horizontal extent of a box also indicates the horizontal scale of the mode.

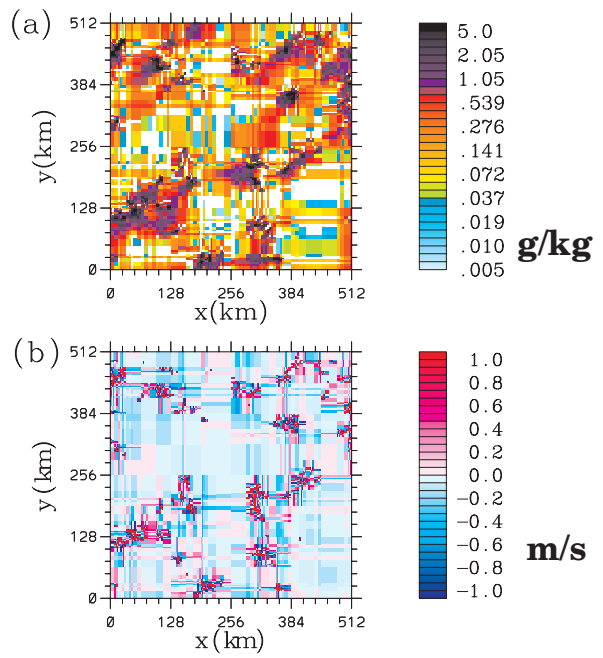

Figure 6. (a) The total condensate (g kg^{-1}), (b) the vertical velocity (m s^{-1}) fields for the TOGA case at 5 km height, approximated by Haar-wavelet decompositions retaining only 1% of the leading components.

these constitute a stepwise logical reduction from the truncated system (3.7), accuracies of the introduced approximations and hypotheses can also be directly verified from the originally full system (3.1). In this manner, mode decomposition provides a framework for systematic developments and verifications of subgrid-scale representations.

(*b*) *The mass-flux based approach*

The mass-flux formulation is an example of mode decomposition based on an idea of dividing the total model domain into horizontal subdomains where physical variables are approximately distributed homogeneously. The main advantage of this approach is that, by using a set of modes with non-vanishing domain-mean values, contributions of subcomponents (e.g. convective and stratiform contributions) to a domain-mean quantity (e.g. condensation rate, precipitation) can easily be computed.

By casting the mass-flux formulation within a general framework of mode decomposition, wider possibilities of this approach are also revealed. By following the systematic reduction from Eq. (3.1) to Eq. (3.7) as outlined in section 3(c), various physical processes can be more systematically introduced into the mass-flux formulation than hitherto envisioned. More remarkably, the mass-flux formulation does not require any closure, when this is adopted as a prognostic representation (Eqs. (4.1) and (4.3)). This prognostic version is akin to earlier attempts at modelling moist deep convection before the invention of the mass-flux formulation (Kasahara and Asai 1967; Asai and Kasahara 1967).

Standard mass-flux based parametrizations are obtained by further reductions from Eqs. (4.1) and (4.3) as outlined in section 4(d). If such a reduction is performed in a logical stepwise manner, the derived parametrization can be directly verified by time integrations of the fully prognostic version (Eqs. (4.1) and (4.3)). This possibility must seriously be considered in future verifications of mass-flux based parametrizations.

However, due to the lack of the admissibility, the mass-flux decomposition cannot be directly performed on a CRM, hence the terms in Eqs. (4.1) and (4.3) cannot directly be evaluated from a CRM. A common practice, to apply a columnwise classification into cloud types (cf. section 4(f)), must be employed only with caution, because this often does not satisfy the segmentally constant approximation to any degree (cf. Guichard *et al.* 1997; Yano *et al.* 2004a).

(*c*) *The wavelet-based approach*

The decomposition based on discrete orthogonal wavelets allows a more systematic reduction of the full system (3.1) into a compressed *prognostic* representation (3.7). Conversely, any subgrid-scale representation based on this framework can directly be verified with the original dynamical system by its decomposition into the same formulation. A working version of a wavelet-based convective representation is still to be developed, but its feasibility is supported by the preliminary energy-cycle analysis presented in section 5(g).

We can make certain analogies in order to intuitively understand the proposed wavelet-based representation of the subgrid-scale processes under a severe truncation of a full system. Lorenz's model for strange attractors (Lorenz 1963) may be the best known example in dynamic meteorology that follows this strategy. He took the Rayleigh–Bénard convection system in Fourier space, whereas we take a CRM in wavelet space. Importantly, both Fourier and the wavelet share much of their mathematical structures as emphasized in section 3. However, as a major difference, the truncation is made *sparse* in wavelet space by retaining only the significant modes regardless of

their scales. The wavelet modes are added locally at appropriate scales in which active convective systems are developing, whereas the wavelet modes are deactivated locally where the amplitude of the disturbance has fallen below a threshold. With a continuous activation and deactivation of modes (cf. Schneider *et al.* 1997), one can efficiently represent the subgrid-scale processes by keeping the required number of modes to a minimum at any instant.

The authors have already tested this wavelet-based approach with simple prognostic partial differential systems (e.g. the Korteweg–de Vries equation, the shallow-water system), and have begun to construct an anelastic system in wavelet space.

ACKNOWLEDGEMENTS

Jean-Pierre Chaboureau has diligently prepared output data sets for the analysis in section 5(g). JIY also acknowledges discussions with Jean-Yves Grandpeix, Akira Kasahara, Jean-Philippe Lafore, Jim McWilliams, Joe Tribbia, a careful reading of the draft by Anton Beljaars, and constructive comments by two anonymous reviewers. Finally but not least, the communications with Akio Arakawa have significantly contributed to improving our understanding of the concept of the mass fluxes.

APPENDIX

Energy cycle of CRMs

Energy integration can be performed on the anelastic system that describes CRMs, along the lines outlined in Holton (1992), for example. Note that Meso-NH employed in the present study adopts its particular version from that developed by Durran (1989).

Under the energy cycle obtained from this integration, the development of convection is described by the conversion C of the available potential energy P into a vertical component K_{V} of the kinetic energy. The two energy components are defined by

$$P = (\rho^* g/\overline{\theta_{\mathrm{v}}})(\theta_{\mathrm{v}}'^2/2)/(\mathrm{d}\overline{\theta_{\mathrm{v}}}/\mathrm{d}z), \tag{A.1}$$

$$K_{\mathrm{V}} = \rho^* w^2/2, \tag{A.2}$$

and the conversion rate C is given by

$$C = \rho^* g \frac{\theta_{\mathrm{v}}' w}{\overline{\theta_{\mathrm{v}}}}. \tag{A.3}$$

Here, $\rho^* = \overline{\rho}\overline{\theta_{\mathrm{v}}}/\theta_0$ is an effective density (cf. Eq. (2) of Durran 1989), w the vertical velocity, g the acceleration of gravity, θ_{v} the virtual potential temperature, and $\theta_0 =$ 300 K. The overbar designates the reference vertical profile of a given variable, and the prime indicates its deviation.

The corresponding expressions in wavelet space are obtained with the help of the Parseval formula (3.10):

$$\widetilde{P}_l = (\rho^* g/\overline{\theta_{\mathrm{v}}})(\widetilde{\theta}_{\mathrm{v},l}'^2/2)/(\mathrm{d}\overline{\theta_{\mathrm{v}}}/\mathrm{d}z), \tag{A.4}$$

$$\widetilde{K}_{\mathrm{V},l} = \rho^* \widetilde{w}_l^2/2, \tag{A.5}$$

$$\widetilde{C}_l = \rho^* g \frac{\widetilde{\theta}_{\mathrm{v},l}' \widetilde{w}_l}{\overline{\theta_{\mathrm{v}}}}, \tag{A.6}$$

where the tilde indicates the wavelet transform. Quantities (A.5), (A.6), (A.4) are plotted in Figs. 5(a), (b), (c), respectively, after integration over the whole vertical domain using the Meyer wavelet.

REFERENCES

Alexander, G. D. and Cotton, W. R. 1998 The use of cloud-resolving simulations of mesoscale convective systems to build a mesoscale parameterization scheme. *J. Atmos. Sci.*, **55,** 2137–2161

Andrews, D. G. and McIntyre, M. E. 1978a Generalized Eliassen–Palm and Charney–Drazin theorems for waves on axisymmetric mean flows in compressible atmospheres. *J. Atmos. Sci.*, **35,** 175–185

1978b An exact theory of nonlinear waves on a Lagrangian-mean flow. *J. Fluid Mech.*, **89,** 609–646

1978c On wave-action and its relatives. *J. Fluid Mech.*, **89,** 647–664

Arakawa, A. 2004 The cumulus parameterization problem: Past, present, and future. *J. Climate*, **17,** 2493–2525

Arakawa, A. and Schubert, W. H. 1974 Interaction of a cumulus cloud ensemble with the large-scale environment, part I. *J. Atmos. Sci.*, **31,** 674–701

Asai, T. and Kasahara, A. 1967 A theoretical study of the compensating downward motions associated with cumulus clouds. *J. Atmos. Sci.*, **24,** 487–496

Bechtold, P., Bazile, E., Guichard, F., Mascart, P. and Richard, E. 2001 A mass-flux convection scheme for regional and global models. *Q. J. R. Meteorol. Soc.*, **127,** 869–886

Bougeault, P. 1985 A simple parameterization of the large-scale effects of cumulus convection. *Mon. Weather Rev.*, **113,** 2108–2121

Browning, K. A., Betts, A., Jonas, P. R., Kershaw, R., Manton, M., Mason, P. J., Miller, M., Moncrieff, M. W., Sundqvist, H., Tao, W. K., Tiedtke, M., Hobbs, P. V., Mitchell, J., Raschke, E., Stewart, R. E., Simpson, J. and Burks, J. E. 1993 The GEWEX Cloud System Study (GCSS). *Bull. Am. Meteorol. Soc.*, **74,** 387–399

Chaboureau, J.-P., Guichard, F., Redelsperger, J.-L. and Lafore, J.-P. 2004 The role of stability and moisture in the diurnal cycle of convection over land. *Q. J. R. Meteorol. Soc.*, **130,** 3105–3117

Churchill, D. D. and Houze, R. A., Jr. 1984 Development and structure of winter monsoon cloud clusters on 10 December 1978. *J. Atmos. Sci.*, **41,** 933–960

Donner, L. J., Seman, C. J. and Hemler, R. S. 1999 Three-dimensional cloud-system modeling of GATE convection. *J. Atmos. Sci.*, **56,** 1885–1912

Durran, D. R. 1989 Improving the anelastic approximation. *J. Atmos. Sci.*, **46,** 1453–1461

Grabowski, W. W. and Smolarkiewicz, P. K. 1999 CRCP: a cloud resolving convection parameterization for modeling the tropical convecting atmosphere. *Physica D*, **133,** 171–178

Grabowski, W. W., Wu, X. and Moncrieff, M. W. 1996 Cloud-resolving modeling of tropical cloud systems during phase III of GATE. Part I: Two-dimensional experiments. *J. Atmos. Sci.*, **53,** 3684–3709

Grabowski, W. W., Wu, X., Moncrieff, M. W. and Hall, W. D. 1998 Cloud-resolving modeling of tropical cloud systems during phase III of GATE. Part II: Effects of resolution and the third spatial dimension. *J. Atmos. Sci.*, **55,** 3264–3282

Grant, A. L. M. and Brown, A. R. 1999 A similarity hypothesis for shallow-cumulus transports. *Q. J. R. Meteorol. Soc.*, **125,** 1913–1936

Grant, A. L. M. and Lock, A. P. 2004 The turbulent kinetic energy budget for shallow cumulus convection. *Q. J. R. Meteorol. Soc.*, **130,** 401–422

Gray, M. E. B. 2000 Characteristics of numerically simulated mesoscale convective systems and their application to parameterization. *J. Atmos. Sci.*, **57,** 3953–3970

Gregory, D. and Guichard, F. 2002 Aspects of the parametrization of organized convection: Contrasting cloud-resolving model and single-column realizations. *Q. J. R. Meteorol. Soc.*, **128,** 625–646

Gregory, D. and Miller, M. J. 1989 A numerical study of the parametrization of deep tropical convection. *Q. J. R. Meteorol. Soc.*, **115,** 1209–1241

Gregory, D. and Rowntree, P. R. 1990 A mass flux convection scheme with representation of cloud ensemble characteristics and stability-dependent closure. *Mon. Weather Rev.*, **118,** 1483–1506

Guichard, F., Lafore, J.-P. and Redelsperger, J.-L. 1997 Thermodynamical impact and internal structure of a tropical convective cloud system. *Q. J. R. Meteorol. Soc.*, **123,** 2297–2324

Guichard, F., Redelsperger, J.-L. and Lafore, J.-P. 2000 Cloud-resolving simulation of convective activity during TOGA-COARE: Sensitivity to external sources of uncertainties. *Q. J. R. Meteorol. Soc.*, **126,** 3067–3095

Holton, J. R. 1992 *An introduction to dynamic meteorology* (*International Geophysical Series*, Vol. 48), 3rd edn., Academic Press, San Diego, USA

Houze, R. A., Jr. 1977 Structure and dynamics of a tropical squall-line system. *Mon. Weather Rev.*, **105,** 1540–1567

1989 Observed structure of mesoscale convective systems and implications for large-scale heating. *Q. J. R. Meteorol. Soc.*, **115,** 425–461

Houze, R. A., Jr. and Betts, A. K. 1981 Convection in GATE. *Rev. Geophys. Space Phys.*, **19,** 541–576

Kasahara, A. and Asai, T. 1967 Effects of an ensemble of convective elements on the large-scale motions of the atmosphere. *J. Meteorol. Soc. Jpn*, **45,** 280–291

Khairoutdinov, M. F. and Randall, D. A. 2002 Similarity of deep continental cumulus convection as revealed by a three-dimensional cloud-resolving model. *J. Atmos. Sci.*, **59,** 2550–2566

Kuo, H. L. 1974 Further studies of the parameterization of the influence of cumulus convection on large-scale flow. *J. Atmos. Sci.*, **31,** 1232–1240

Lafore, J.-P., Redelsperger, J.-L. and Jaubert, G. 1988 Comparison between a three-dimensional simulation and doppler radar data of a tropical squall line: Transports of mass, momentum, heat, and moisture. *J. Atmos. Sci.*, **45,** 3483–3500

Lafore, J. P., Stein, J., Asencio, N., Bougeault, P., Ducrocq, V., Duron, J., Fischer, C., Héreil, P., Mascart, P., Masson, V., Pinty, J. P., Redelsperger, J.-L., Richard, E. and de Arellano, J. V.-G. 1998 The Meso-NH atmospheric simulation system. Part I: adiabatic formulation and control simulations. *Ann. Geophys.*, **16,** 90–109

Lorenz, E. N. 1963 Deterministic nonperiodic flow. *J. Atmos. Sci.*, **20,** 130–148

Mallat, S. 1998 *A wavelet tour of signal processing*. 2nd edn., Academic Press

Mellor, G. L. and Yamada, T. 1974 A hierarchy of turbulence closure models for planetary boundary layers. *J. Atmos. Sci.*, **31,** 1791–1806

Moncrieff, M. W. 1995 Mesoscale convection from a large-scale perspective. *Atmos. Res.*, **35,** 87–112

Moncrieff, M. W., Krueger, S. K., Gregory, D., Redelsperger, J.-L. and Tao, W.-K. 1997 GEWEX Cloud System Study (GCSS) Working Group 4: Precipitating convective cloud systems. *Bull. Am. Meteorol. Soc.*, **78,** 831–845

Ooyama, K. V. 1971 A theory on parameterization of cumulus convection. *J. Meteorol. Soc. Jpn*, **49,** 744–756

Randall, D. A., Khairoutdinov, M., Arakawa, A. and Grabowski, W. 2003 Breaking the cloud parameterization deadlock. *Bull. Am. Meteorol. Soc.*, **84,** 1547–1564

Redelsperger, J.-L., Brown, P. R. A., Guichard, F., Hoff, C., Kawasima, M., Lang, S., Montmerle, T., Nakamura, K., Saito, K., Seman, C., Tao, W.-K. and Donner, L. J. 2000 A GCSS model intercomparison for a tropical squall line observed during TOGA-COARE. I: Cloud-resolving models. *Q. J. R. Meteorol. Soc.*, **126,** 823–863

Rutledge, S. A. 1991 Middle latitude and tropical mesoscale convective systems. *Rev. Geophys. Suppl.*, **29,** 88–97

Schneider, K., Kevlahan, N. K.-R. and Farge, M. 1997 Comparison of an adaptive wavelet method and nonlinearly filtered pseudospectral methods for two-dimensional turbulence. *Theoret. Comput. Fluid Dynamics*, **9,** 191–206

Soong, S.-T. and Tao, W.-K. 1980 Response of deep tropical cumulus clouds to mesoscale processes. *J. Atmos. Sci.*, **37,** 2016–2034

Steiner, M. S., Houze, R. A., Jr. and Yuter, S. E. 1995 Climatological characterization of three-dimensional storm structure from operational radar and rain gauge data. *J. Appl. Meteorol.*, **34,** 1978–2007

Stull, R. B. 1993 Review of non-local mixing in turbulent atmospheres: Transilient turbulence theory. *Boundary-Layer Meteorol.*, **62,** 21–96

Sui, C.-H., Lau, K. M., Tao, W.-K. and Simpson, J.	1994	The tropical water and energy cycles in a cumulus ensemble model. Part I: equilibrium climate. *J. Atmos. Sci.*, **51,** 711–728
Tao, W.-K. and Simpson, J.	1989	Modeling study of a tropical squall-type convective line. *J. Atmos. Sci.*, **46,** 177–202
Tiedtke, M.	1989	A comprehensive mass flux scheme of cumulus parameterization in large-scale models. *Mon. Weather Rev.*, **117,** 1779–1800
Wu, X. and Moncrieff, M. W.	2001	Long-term behavior of cloud systems in TOGA COARE and their interactions with radiative and surface processes. Part III: Effects on the energy budget and SST. *J. Atmos. Sci.*, **58,** 1155–1168
Wu, X., Grabowski, W. W. and Moncrieff, M. W.	1998	Long-term behavior of cloud systems in TOGA COARE and their interactions with radiative and surface processes. Part I: Two-dimensional modeling study. *J. Atmos. Sci.*, **55,** 2693–2714
Wu, X., Hall, W. D., Grabowski, W. W., Moncrieff, M. W., Collins, W. D. and Kiehl, J. T.	1999	Long-term behavior of cloud systems in TOGA COARE and their interactions with radiative and surface processes. Part II: Effects of ice microphysics on cloud-radiation interaction. *J. Atmos. Sci.*, **56,** 3177–3195
Xie, S., Xu, K.-M., Cederwall, R. T., Bechtold, P., Del Genio, A. D., Klein, S. A., Cripe, D. G., Ghan, S. J., Gregory, D., Iacobellis, S. F., Krueger, S. K., Lohmann, U., Petch, J. C., Randall, D. A., Rotstayn, L. D., Somerville, R. C. J., Sud, Y. C., Von Salzen, K., Walker, G. K., Wolf, A., Yio, J. J., Zhang, G. J. and Zhang, M.	2002	Intercomparison and evaluation of cumulus parametrizations under summertime midlatitude continental conditions. *Q. J. R. Meteorol. Soc.*, **128,** 1095–1135
Xu, K.-M.	1994	A statistical analysis of the dependency of closure assumptions in cumulus parameterization on the horizontal resolution. *J. Atmos. Sci.*, **51,** 3674–3691
	1995	Partitioning mass, heat, and moisture budgets of explicitly simulated cumulus ensembles into convective and stratiform components. *J. Atmos. Sci.*, **52,** 551–573
Xu, K.-M. and Arakawa, A.	1992	Semiprognostic tests of the Arakawa–Schubert cumulus parameterization using simulated data. *J. Atmos. Sci.*, **49,** 2421–2436
Xu, K.-M. and Randall, D. A.	1996	Explicit simulation of cumulus ensembles with the GATE Phase III data: Comparison with observations. *J. Atmos. Sci.*, **53,** 3710–3736
	2000	Explicit simulation of midlatitude cumulus ensembles: Comparison with ARM data. *J. Atmos. Sci.*, **57,** 2839–2858
	2001	Updraft and downdraft statistics of simulated tropical and midlatitude cumulus convection. *J. Atmos. Sci.*, **58,** 1630–1649
Xu, K.-M., Arakawa, A. and Krueger, S. K.	1992	The macroscopic behavior of cumulus ensembles simulated by a cumulus ensemble model. *J. Atmos. Sci.*, **49,** 2402–2420
Xu, K.-M., Cederwall, R. T., Donner, L. J., Grabowski, W. W., Guichard, F., Johnson, D. E., Khairoutdinov, M., Krueger, S. K., Petch, J. C., Randall, D. A., Seman, C. J., Tao, W.-K., Wang, D., Xie, S. C., Yio, J. J. and Zhang, M.-H.	2002	An intercomparison of cloud-resolving models with the Atmospheric Radiation Measurement summer 1997 Intensive Observation Period data *Q. J. R. Meteorol. Soc.*, **128,** 593–624
Yanai, M. and Johnson, R. H.	1993	'Impacts of cumulus convection on thermodynamic fields'. Pp. 39–62 in *The representation of cumulus convection in numerical models.* Meteorol. Mono., Vol. 46, American Meteorological Society
Yanai, M., Esbensen, S. and Chu, J.-H.	1973	Determination of bulk properties of tropical cloud clusters from large-scale heat and moisture budgets. *J. Atmos. Sci.*, **30,** 611–627

Yano, J.-I. 2004 'The cumulus parameterization problem in the context of MJO simulations'. Proceedings of the MJO workshop, ECMWF, 3–6 November 2003, pp. 115–128. http://www.ecmwf.int/publications/library/do/references/list/17124

Yano, J.-I., Moncrieff, M. W., Wu, X. and Yamada, M. 2001a Wavelet analysis of simulated tropical convective cloud systems. Part I: Basic analysis. *J. Atmos. Sci.*, **58,** 850–867

Yano, J.-I., Moncrieff, M. W. and Wu, X. 2001b Wavelet analysis of simulated tropical convective cloud systems. Part II: Decomposition of convective-scale and mesoscale structure. *J. Atmos. Sci.*, **58,** 868–876

Yano, J.-I., Bechtold, P. and Redelsperger, J.-L. 2003 'Renormalization' approach for subgrid-scale representations. *J. Atmos. Sci.*, **60,** 2029–2038

Yano, J.-I., Guichard, F., Lafore, J.-P., Redelsperger, J.-L. and Bechtold, P. 2004a Estimations of mass fluxes for cumulus parameterizations from high-resolution spatial data. *J. Atmos. Sci.*, **61,** 829–842

Yano, J.-I., Bechtold, P., Redelsperger, J.-L. and Guichard, F. 2004b Wavelet-compressed representation of deep moist convection. *Mon. Weather Rev.*, **132,** 1472–1486

Yano, J.-I., Chaboureau, J.-P. and Guichard, F. 2005 A generalization of CAPE into potential-energy convertibility. *Q. J. R. Meteorol. Soc.*, **131,** 861–875